Experimental Investigation on the Effect of Roller Traverse and Rotation Speeds on Ceramic Binder Jetting Additive Manufacturing

Guanxiong Miaoa, Mohammadamin Moghadasib, Wenchao Duc, Zhijian Peic, Chao Maa,b,c,d,*

a Department of Mechanical Engineering, Texas A&M University, College Station, TX, US

^b Department of Material Science and Engineering, Texas A&M University, College Station, TX, US

^c Department of Industrial and Systems Engineering, Texas A&M University, College Station, TX, US

^d Department of Engineering Technology and Industrial Distribution, Texas A&M University, College

Station, TX, US

* Corresponding author: cma@tamu.edu (Chao Ma). 3367 TAMU, College Station, TX 77843, USA

Keywords: Binder jetting, Roller traverse speed, Roller rotation speed

Abstract

The objective of this experimental investigation is to identify the effect of roller traverse and rotation

speeds on ceramic binder jetting additive manufacturing. Green and sintered densities were found

decreasing with increasing roller traverse speed, and this decrease was more significant at a low roller

rotation speed. A high roller traverse speed led to more cavities on the powder bed surface after

spreading a new layer on a printed layer. Furthermore, a high roller traverse speed caused more cracks

on the powder bed surface after jetting the binder. These defects observed during printing were inherited

by the green and sintered parts, which were confirmed by X-ray computed tomography and scanning

electron microscopy, respectively. Finally, the sintered flexural strength of the parts printed at a high roller

traverse speed was more than 30% higher than that of the parts printed at a low roller traverse speed.

1

1. Introduction

Binder jetting is one of the seven major additive manufacturing technologies defined by ASTM [1]. Compared with other additive manufacturing technologies, binder jetting is advantageous in printing complex geometries [2, 3]. No explicit support is needed for overhangs because the powder bed acts as the support and there is no thermal stress during the printing process [3, 4]. The other advantageous of binder jetting include high flexibility for the feedstock material and high scalability [4-12].

Powder spreading is a critical step of binder jetting since the quality of the spread powder layers could affect the printing and sintering processes, and thus, affect the quality of the green and sintered parts [12-14]. Counter-rotating roller has been widely used in binder jetting to spread powder because the rotation of the counter-rotating roller could improve powder spreading [15-17]. However, this is only true when the appropriate traverse and rotation speeds are selected.

Several studies on selecting a proper roller traverse speed have been reported. Miyanaji et al. printed dental porcelain powder at two roller traverse speeds, and the results suggested that a low traverse speed was desired for forming a uniform and dense powder layer but could deteriorate the dimensional accuracy in the X direction [18, 19]. Another experimental work by Miyanaji et al. showed a different trend: a high roller traverse speed resulted in dense parts for fine cooper powder [20]. Sanjay et al. printed 316L stainless steel powder at three different roller traverse speeds and found that a low traverse speed could result in a high rupture strength [21]. However, the focus of these studies was optimizing process parameters instead of studying the effect of roller traverse speed. To better understand how roller traverse speed affects binder jetting, this work involved a systematic study on the effect of roller traverse speed. Green and sintered densities of the parts printed at a wide range of roller traverse speeds were examined. Powder bed surface, green microstructure, sintered microstructure, and sintered flexural strength at selected low and high roller traverse speeds were further characterized.

In addition to roller traverse speed, roller rotation speed also affects powder spreading [15, 22-24]. However, the influence of roller rotation is unclear. The experimental work by Meyer et al. showed the total surface velocity (i.e., the sum of rotation speed and traverse speed) was a better predictor of the

powder bed density than roller traverse or rotation speed individually [25]. The experimental work by Rishmawi et al. demonstrated the main effect of traverse or rotation speed individually was stronger than the interaction effect of these two parameters [26]. To determine how the roller rotation speed interacts with roller traverse speed, experiments at three roller rotation speeds were also carried out in this work.

2. Experimental methods

2.1 Powder material

Alumina-based ceramic powder (Tethonite High Alumina Ceramic Powder, TETHON 3D, USA) was used as the raw material for this study. The morphology and particle size distribution of the powder were characterized with a scanning electron microscope (JSM–7500F, JEOL, Japan) and a laser scattering machine (LA–960, HORIBA, Japan), respectively. Figure 1 (a) shows the irregular particle shape, and Figure 1 (b) shows the wide particle size distribution (i.e., from below 10 μm to more than 100 μm).

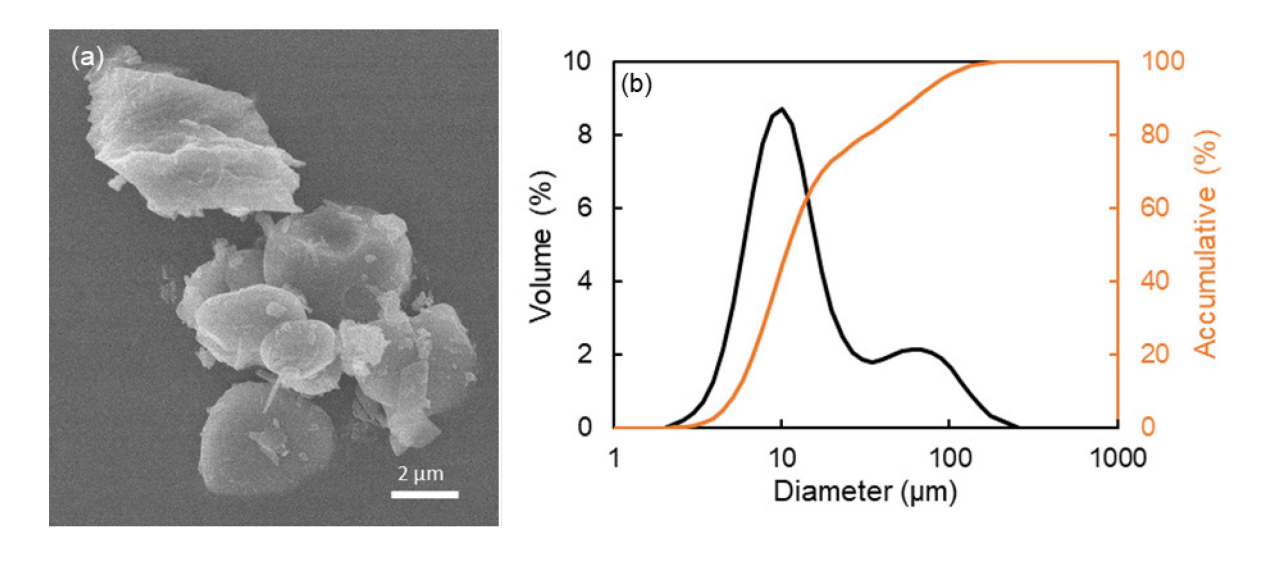


Figure 1. (a) Morphology and (b) particle size distribution of the powder

2.2 Printing and post-processing

A commercially available binder jetting 3D printer (Innovent+, ExOne, USA) was used to study the effect of roller traverse and rotation speeds in this work. Eight roller traverse speeds and three roller rotation speeds were tested to form a full factorial design. To cover a wide range of roller traverse speeds, the eight roller traverse speeds were selected between the lowest traverse speed allowed on this printer (i.e.,

1 mm/s) and the highest traverse speed that could lead to a successful print in the preliminary experiments (i.e., 200 mm/s). The three roller rotation speeds were selected within the range that led to a successful print in the preliminary experiments (i.e., 150, 300, and 450 RPM). Besides the roller traverse and rotation speeds, the other process parameters (listed in Table 1) were selected based on preliminary experiments and were kept the same for all the experiments. For each combination of roller traverse and rotation speeds, 15 square prisms (shown in Figure 2) were printed. The length and width of the prisms were 10 mm, and the height (along the Z direction of the printer) of the prisms was 12.5 mm.

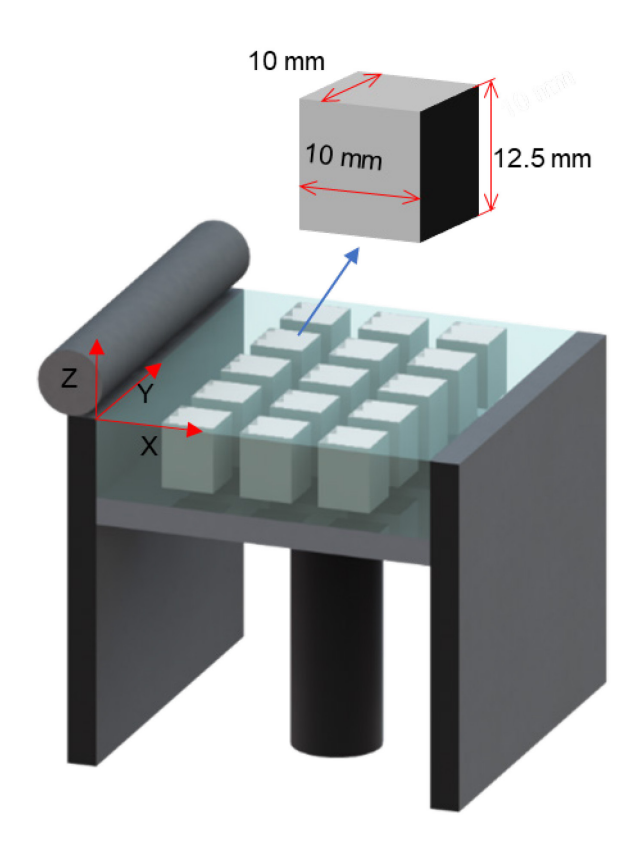


Figure 2. Printing layout and the design of test prism

Table 1. Process parameters

Process parameter	Value
Layer thickness (µm)	200
Ultrasonic intensity (%)	100
Roller traverse speed (mm/s)	1, 2, 5, 10, 20, 50, 100, 200
Roller rotation speed (RPM)	150, 300, 450
Roughing roller rotation speed (RPM)	50
Binder saturation (%)	70
Binder set time (s)	20
Bed temperature (°C)	50
Drying time (s)	10

After printing, all the green parts were cured in a furnace (DX402C, Yamato Scientific America, USA) at 200 °C for 4 hours. Then six parts were randomly selected from each print and were moved to a muffle furnace (KSL–1700X, MTI, USA) for debinding at 480 °C for about 3 hours and sintering at 1700 °C for about 2 hours following the profile plotted in Figure 3. All post-processing steps (curing, debinding, and sintering) were performed in air.

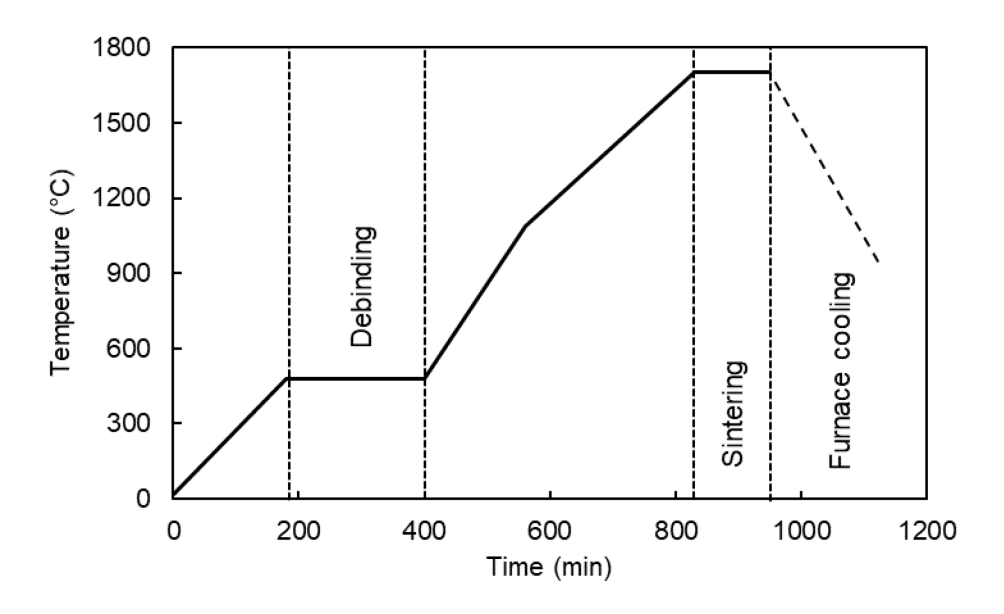


Figure 3. Debinding and sintering profile

2.3 Green and sintered densities measurement

In this work, both green and sintered densities were used to evaluate the performance of different combinations of roller traverse and rotation speeds. After curing, green density was measured for all the 15 parts in each print using the geometric method: the mass of the green parts was measured using a scale with a resolution of 0.001 g and the dimensions were measured using a caliper with a resolution of 0.01 mm. Sintered (bulk) density was measured for the six sintered parts in each print using the Archimedes' method following the ISO–18754 standard [27]. The measured green and sintered densities were then divided by the theoretical density of the feedstock material (i.e., 3.56 g/cm³) to calculate the relative green and sintered densities. The relative densities were used for all the comparisons and analysis in this work.

2.4 Powder bed surface imaging

A camera (α9, SONY, Japan) was used to photograph the powder bed surface in the prints at the selected low and high roller traverse speeds. Images were taken of three different kinds of layers: the powder layer that was spread on loose powder, the powder layer that was spread on a printed layer, and the printed layer.

2.5 Green microstructure characterization

An X-ray computed tomography (CT) system (X50, NSI, USA) was used to characterize the internal microstructure of the green parts. A camera (α9, SONY, Japan) was used to photograph the surfaces of the green parts. Parts that were printed at the selected low and high roller traverse speeds were characterized. The parts went through curing and depowering without any other treatment before scanning.

2.6 Sintered microstructure characterization

A scanning electron microscope (SEM, FERA–3, TESCAN ANALYTICS, Czech Republic) was used to characterize the internal microstructure of the sintered parts that were printed at the selected low and high roller traverse speeds. To prepare the sintered parts for SEM characterization, the top and side

surface of the sintered parts were lapped first (model 15, LAPMASTER, USA) to reveal the internal structure and then were coated with platinum using a sputter coater (108 Auto, Cressington, UK).

2.7 Sintered flexural strength measurement

To test the sintered flexural strength, test bars specified by the ASTM–C1161 standard [28] were produced at the selected low and high roller traverse speeds. Fifteen test bars were printed for each roller traverse speed, and all the printing parameters were kept the same as that used to print prisms. The length, width, and depth of the test bars were aligned with the Y, X, and Z axes of the printer, respectively. The CAD design of the test bars was enlarged according to the sintering shrinkage measured in the preliminary experiments to make sure the dimensions of the sintered test bars were close to specifications in the standard (i.e., 45×4×3 mm³). Before testing, the four large surfaces of the sintered test bars were lapped to eliminate the random defects on the surface and make sure the final dimensions were within the range specified in the standard. Then, a universal tester (Insight 30, MTS, USA) was used for the three-point flexural test. The measured flexural strength was evaluated using the Weibull statistics.

3. Results and discussion

3.1 The effect of roller traverse and rotation speeds on green and sintered densities

Figure 4 shows the effect of roller traverse and rotation speeds on the green density. The green density is high at a low roller traverse speed and gradually decreases with the increasing roller traverse speed. This decreasing trend holds at all the tested roller rotation speeds, but the decrease is more significant at a low roller rotation speed (i.e., from 25.7% to 19.6% at the rotation speed of 150 RPM) and is less significant at a high roller rotation speed (i.e., from 24.6% to 22.6% at the rotation speed of 450 RPM). The low green density at a high roller traverse speed was probably because the particles had fewer chances to rearrange when spread with a fast-moving roller. By reducing the roller traverse speed, the particles had more time to rearrange, and thus, achieved a higher green density. As for the effect of roller rotation speed, it could be explained from two aspects. Firstly, at a low roller traverse speed, a high roller rotation speed might cause a severe particle circulation in the powder heap [25, 29, 30] which could

prevent particles from being deposited, and thus, led to a green density lower than that achieved at a low rotation speed. Secondly, at a high roller traverse speed, a high roller rotation speed could counteract the negative effect of the high roller traverse speed by helping the particles to rapidly rearrange during a short spreading time to achieve a green density higher than that achieved at a low rotation speed.

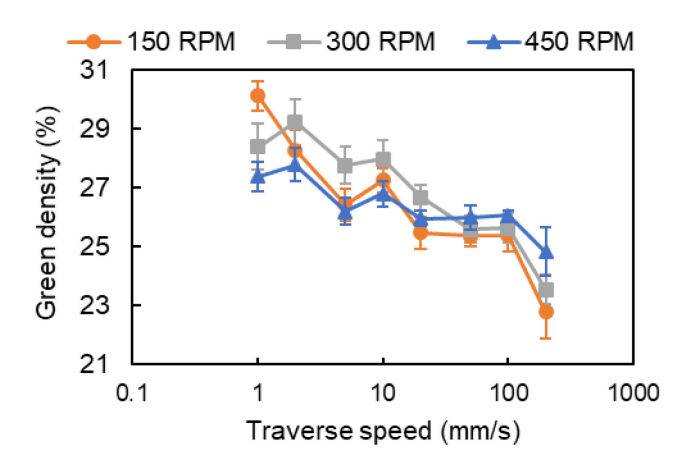


Figure 4. Density of green parts printed at different roller traverse and rotation speeds

The sintered density achieved at different roller traverse and rotation speeds is shown in Figure 5. The sintered density decreases with the increasing roller traverse speed, and the decrease is more significant at a low roller rotation speed. The decreasing trend is similar to what was obtained for the green density, indicating that the green density had a determinative effect on the sintered density and the densification during sintering was not large enough to compensate for the difference between green parts printed at different roller traverse and rotation speeds.

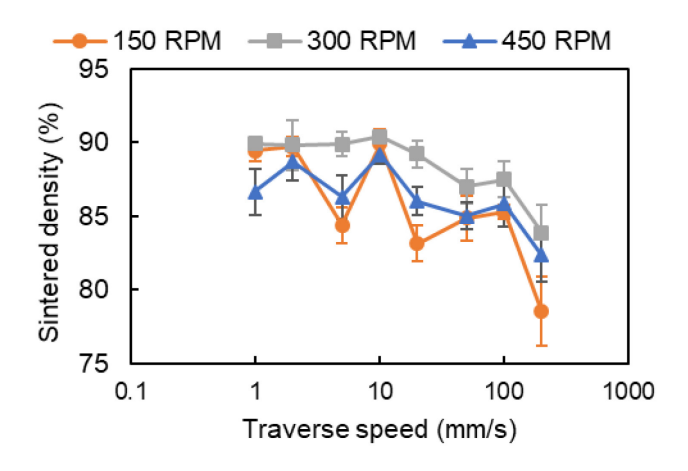


Figure 5. Density of sintered parts printed at different roller traverse and rotation speeds

3.2 Comparison of powder bed surfaces at low and high roller traverse speeds

According to the previous section, roller traverse speed had a more significant effect on printing than the roller rotation speed. Therefore, parts printed at the same roller rotation speed (300 RPM) but different roller traverse speeds (2 mm/s and 200 mm/s) were studied in depth to further reveal the effect of the roller traverse speed.

Figure 6 is a comparison of the powder bed surfaces obtained at the low and high roller traverse speeds. When the powder was spread on loose powder without jetting any binder (Figure 6 (a) and (b)), the powder bed surface created at a high traverse speed was slightly rougher than that created at low traverse speed. Other than that, no significant difference was observed for the powder bed surfaces at the low and high roller traverse speeds.

After a new layer of powder was spread on a printed layer, cavities were found at the high roller traverse speed (Figure 6 (d)). These defects could be caused by the roller dragging agglomerated powder. When a new layer is spread on top of a printed layer, the newly spread powder could absorb the binder from the previously printed layer and become agglomerated. The agglomerated powder could be dragged by the roller when the agglomerate size was comparable to the layer thickness. This dragging effect was more severe when the roller traversed fast due to the lack of rearrangement.

Figures 6 (e) and (f) are the powder bed surfaces immediately after binder was jetted. Periodic cracks along Y direction are readily visible at both traverse speeds. The distance between two adjacent cracks matched the distance between two adjacent nozzles on the print head, which meant the cracks were caused by the jetted binder. When penetrating the powder bed, the binder might have caused powder to sink and form the cracks. The cracks in Figure 6 (f) are more continuous than those in Figure 6 (e). This is probably because at the higher traverse speed, the powder packing density is lower, and thus, the powder sinks more. This mechanism is more evident by observing the boundaries between the printed and unprinted areas in Figures 6(e) and (f). The boundaries are clearer in Figure 6(f) than those in Figure 6(e).

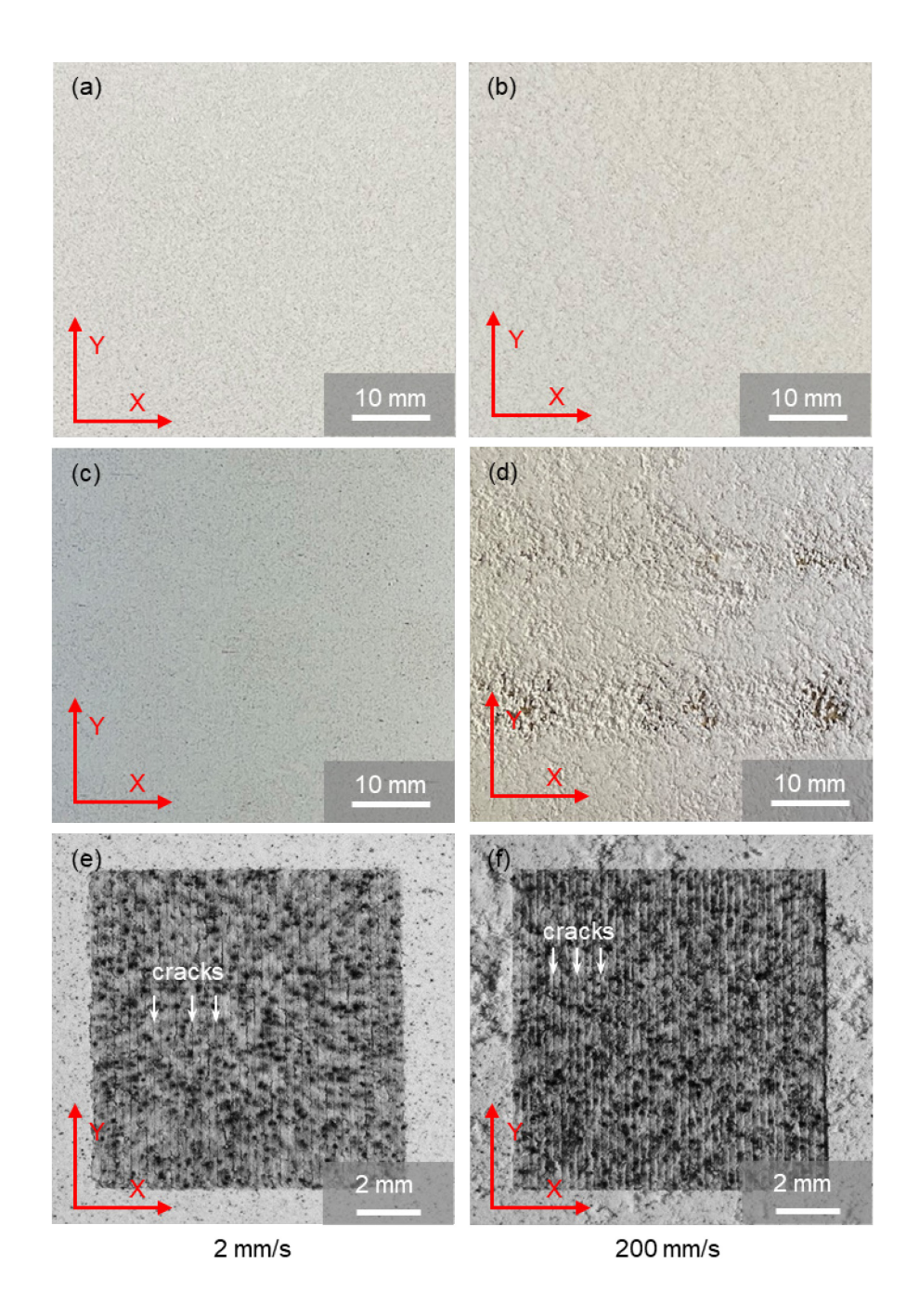


Figure 6. Powder bed surfaces obtained at different traverse speeds (2 mm/s and 200 mm/s): (a) (b) a newly spread layer (before jetting binder) on loose powder, (c) (d) a newly spread layer (before jetting binder) on a printed layer, and (e) (f) a printed layer

3.3 Comparison of green microstructures at low and high roller traverse speeds

After curing, the periodic cracks discussed in the previous section were still evident on the top surface of the green parts (Figure 7 (a) and (b)). In addition, the layered structure was visible on the YZ side

surfaces of the green parts (Figure 7 (c) and (d)), which indicated the defects were present between layers. Compared with the part printed at the low roller traverse speed (2 mm/s), the layered structure was more significant for the part printed at the high roller traverse speed (200 mm/s).

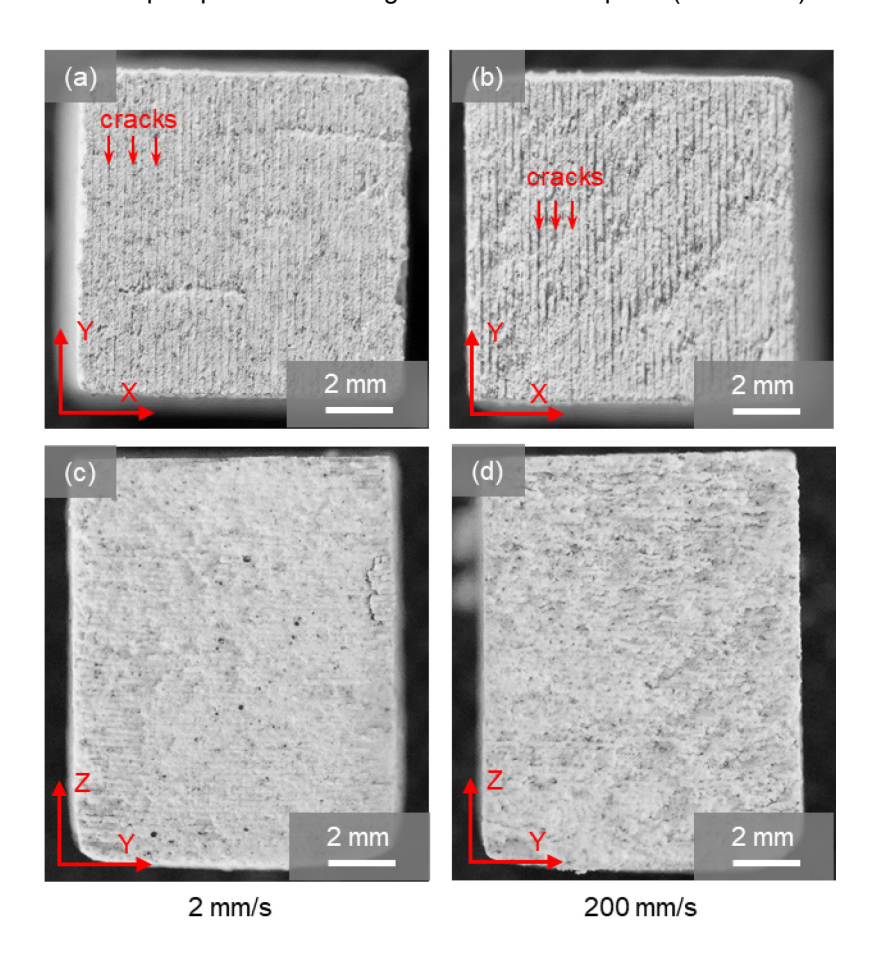


Figure 7. Optical images of surfaces of green parts printed at different roller traverse speeds (2 mm/s and 200 mm/s): (a) (b) top surface and (c) (d) YZ side surface

To better identify the number and distribution of the defects, X-ray CT was used to characterize the internal structure of the green parts. Figure 8 (a) and (b) are cross sections parallel to the top surface. For the part printed at the roller traverse speed of 2 mm/s, the cracks caused by the binder were still visible in the middle of the part (Figure 8 (a)) but was not as obvious as that on the top surface (Figure 7(a)), indicating that the cracks did not penetrate deep into the powder layer because of the high powder packing density. As for the part printed at the roller traverse speed of 200 mm/s, these cracks were still evident in the middle of the part, which suggested that the cracks extended through the whole layer due to the low powder packing density.

Figure 8 (c) and (d) are YZ cross sections of the green part. Inter-layer defects were significant for parts printed at both low and high roller traverse speeds, and were more significant on the parts printed at the high roller traverse speed. Some defects even spanned several layers for the part printed at the high roller traverse speed. The more defects at the high roller traverse speed indicated that such a high roller traverse speed is not able to spread uniform powder layers, which agrees with the finding in the previous section.

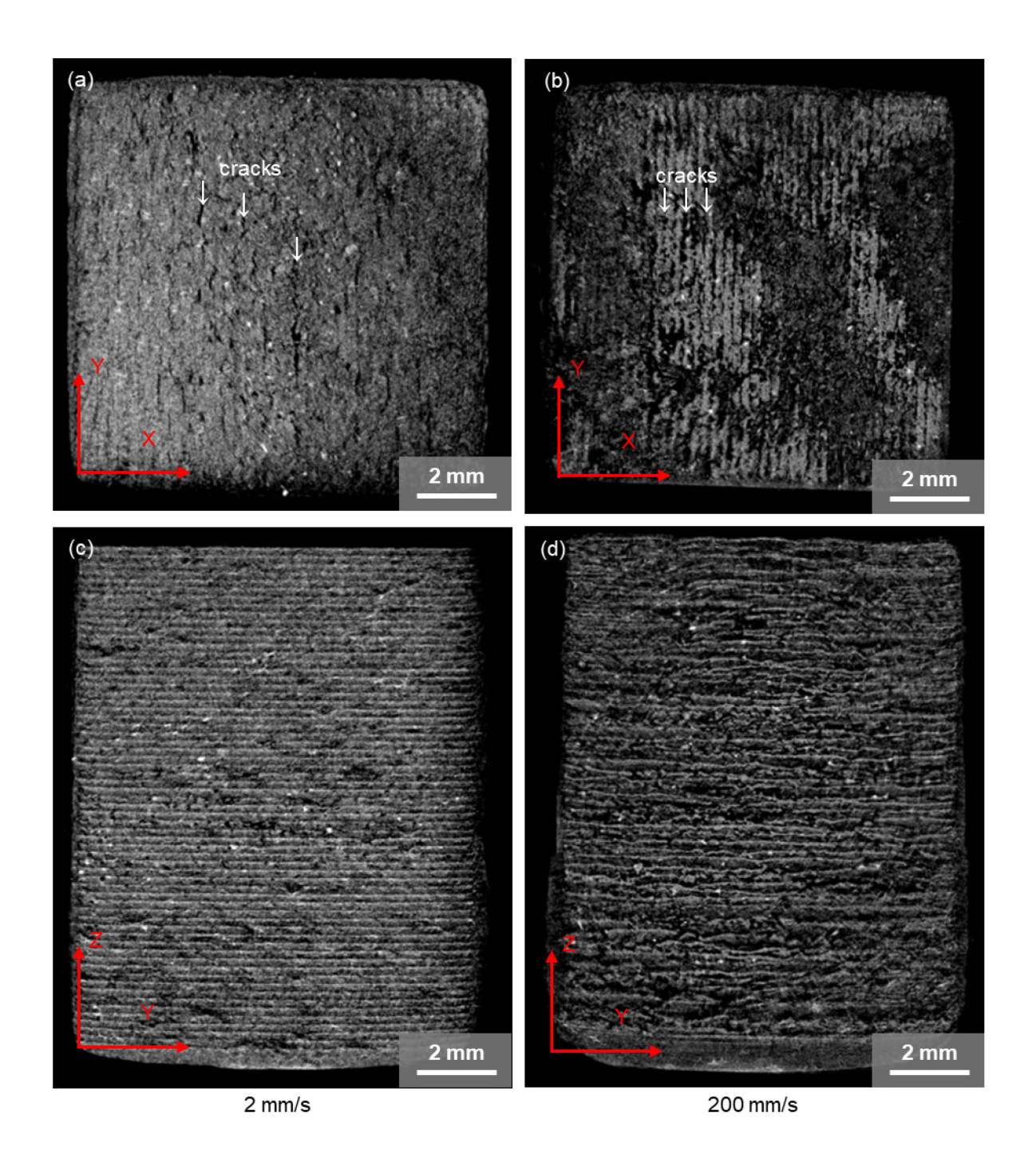


Figure 8. X-ray CT images of internal structures of green parts printed at different roller traverse speeds (2 mm/s and 200 mm/s): (a) (b) XY cross sections and (c) (d) YZ cross sections

3.4 Comparison of sintered microstructures at low and high roller traverse speeds

Internal microstructures of the sintered parts were characterized by imaging the lapped parts with SEM.

After sintering, densified microstructure was observed for parts printed at both low and high roller traverse

speeds (2 mm/s and 200 mm/s), which indicated the high sinterability [10] of the feedstock powder.

Defects were observed on both the XY and YZ cross sections. Similar to the powder bed and green parts, the sintered part printed at the high roller traverse speed had more defects than that printed at the low roller traverse speed.

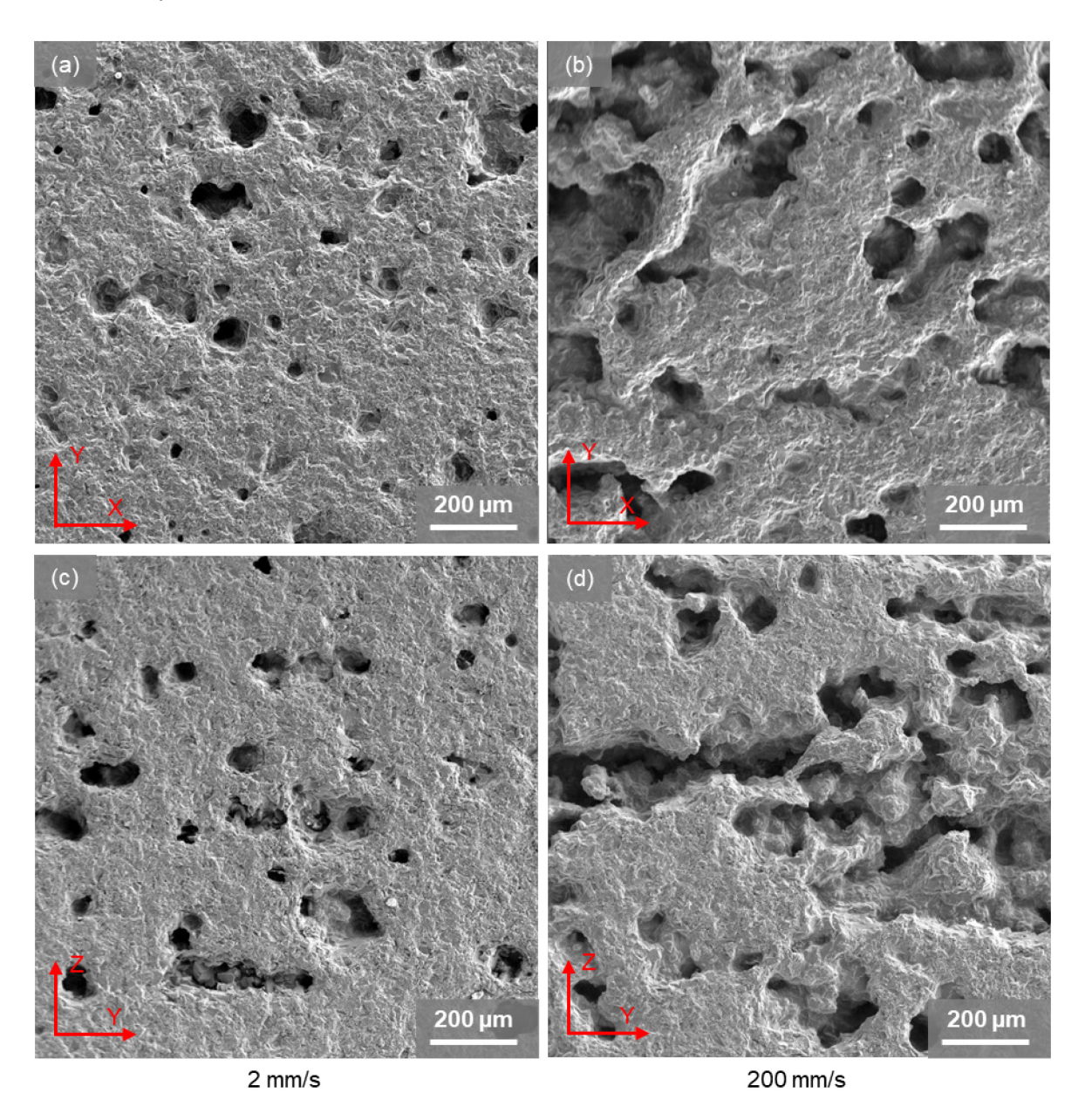


Figure 9. Lapped surface of sintered parts printed at different roller traverse speeds (2 mm/s and 200 mm/s): (a) (b) XY cross sections and (c) (d) YZ cross sections

3.5 Comparison of sintered flexural strengths at low and high roller traverse speeds

Flexural strength was measured for test bars printed at the roller traverse speeds of 2 mm/s and 200 mm/s. Weibull statistics was used to analyze the flexural strength data, as plotted in Figure 10. For test bars printed at the low roller traverse speed, the characteristic strength was 167.5 MPa (90% confidence interval: 162.0–173.4 MPa), and the Weibull modulus was 14.9 (90% confidence interval: 9.5–19.4). For test bars printed at the high roller traverse speed, the characteristic strength was 125.7 MPa (90% confidence interval: 118.5–133.5 MPa), and the Weibull modulus was 7.1 (90% confidence interval: 4.9–9.0). The higher characteristic strength of the test bars printed at the low roller traverse speed indicated that these test bars had a flexural strength higher than that of test bars printed at the high roller traverse speed. The Weibull modulus results suggested that the test bars printed at the low roller traverse speed had a lower variation, and thus, a more consistent part quality than those printed at the high roller traverse speed.

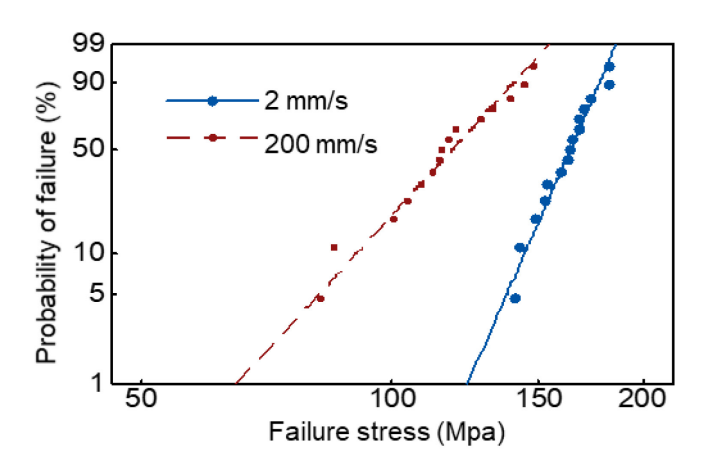


Figure 10. Probability of failure versus failure stress for sintered parts printed at different roller traverse speeds (2 mm/s and 200 mm/s)

4. Concluding remarks

In this work, the effect of the roller traverse and rotation speeds on green and sintered densities was systematically investigated through experiments. Then, to better understand the experimental results, powder bed surface, green microstructure, and sintered microstructure at low and high roller traverse speeds were further characterized. In addition, sintered flexural strength of the parts printed at the low

and high roller traverse speeds was also tested. Based on this work, the following conclusions can be made:

- The green and sintered densities were significantly affected by roller traverse speed. The higher the roller traverse speed, the lower the green and sintered densities.
- The effect of roller traverse speed on densities interacted with the effect of roller rotation speed.
 The effect of roller traverse speed was more significant at a low roller rotation speed.
- There were more defects on the powder bed surface at a high roller traverse speed, especially
 when a layer is spread on a printed layer (compared with the scenario when a layer is spread on
 loose powder).
- Periodical defects along Y direction on the XY plane were found for the powder bed and green
 parts that were printed at both low and high roller traverse speeds. These defects were more
 evident when high roller traverse speeds were used. The distance between two adjacent defects
 matched the distance between two adjacent nozzles on the print head, which indicated that the
 defects were associated with the jetted binder.
- Interlayer defects were found in green parts and sintered parts printed at both low and high roller traverse speeds. There were more interlayer defects when a high roller traverse speed was used.
- The sintered flexural strength was influenced by roller traverse speed. A high roller traverse speed led to a low sintered flexural strength and a high strength variance.

This paper focuses on the effect of roller traverse and rotation speeds on ceramic binder jetting additive manufacturing. However, binder jetting is a complex process involving many other printing parameters. Understanding the effect of other printing parameters is also essential for a successful print and therefore suggested as a future research direction.

Acknowledgement

This material is based upon work supported by the National Science Foundation under Grant No. 1762341.

References

- [1] ISO/ASTM, ASTM52900-15 Standard Terminology for Additive Manufacturing—General Principles—Terminology, ASTM International, West Conshohocken, PA, 2015, p. 5.
- [2] Y. Tang, Y. Zhou, T. Hoff, M. Garon, Y. Zhao, Elastic Modulus of 316 Stainless Steel Lattice Structure Fabricated via Binder Jetting Process, Materials Science and Technology 32(7), 2016, 648-656.
- [3] A. Mostafaei, E.L. Stevens, J.J. Ference, D.E. Schmidt, M. Chmielus, Binder Jetting of a Complex-Shaped Metal Partial Denture Framework, Additive Manufacturing 21, 2018, 63-68.
- [4] M. Ziaee, N.B. Crane, Binder Jetting: A Review of Process, Materials, and Methods, Additive Manufacturing 28, 2019, 781-801.
- [5] M. Li, W. Du, A. Elwany, Z. Pei, C. Ma, Binder Jetting Additive Manufacturing of Metals: A Literature Review, The ASME International Manufacturing Science and Engineering Conference, Erie, PA, US., 2019.
- [6] B. Graybill, M. Li, D. Malawey, C. Ma, J.-M. Alvarado-Orozco, E. Martinez-Franco, Additive Manufacturing of Nickel-Based Superalloys, The ASME International Manufacturing Science and Engineering Conference, College Station, TX, US, 2018.
- [7] W. Du, X. Ren, C. Ma, Z. Pei, Binder Jetting Additive Manufacturing of Ceramics: A Literature Review, The ASME International Mechanical Engineering Congress and Exposition, Tampa, FL, US., 2017.
- [8] L.A. Chavez, P. Ibave, B. Wilburn, D. Alexander, C. Stewart, R. Wicker, Y. Lin, The Influence of Printing Parameters, Post-Processing, and Testing Conditions on the Properties of Binder Jetting Additive Manufactured Functional Ceramics, Ceramics 3(1), 2020, 65-77.
- [9] A. Mostafaei, A.M. Elliott, J.E. Barnes, C.L. Cramer, P. Nandwana, M. Chmielus, Binder Jet 3D Printing–Process Parameters, Materials, Properties, and Challenges, Progress in Materials Science 119, 2021, 100707.
- [10] N. Guo, M.C. Leu, Additive Manufacturing: Technology, Applications and Research Needs, Frontiers of Mechanical Engineering 8(3), 2013, 215-243.
- [11] D. Bourell, J.P. Kruth, M. Leu, G. Levy, D. Rosen, A.M. Beese, A. Clare, Materials for Additive Manufacturing, CIRP Annals 66(2), 2017, 659-681.
- [12] W. Du, X. Ren, Z. Pei, C. Ma, Ceramic Binder Jetting Additive Manufacturing: A Literature Review on Density, Journal of Manufacturing Science and Engineering 142(4), 2020.
- [13] G. Miao, W. Du, M. Moghadasi, Z. Pei, C. Ma, Ceramic Binder Jetting Additive Manufacturing: Effects of Granulation on Properties of Feedstock Powder and Printed and Sintered Parts, Additive Manufacturing, 2020, 101542.
- [14] R. Hebert, Metallurgical Aspects of Powder Bed Metal Additive Manufacturing, Journal of Materials Science 51(3), 2016, 1165-1175.
- [15] S. Haeri, Y. Wang, O. Ghita, J. Sun, Discrete Element Simulation and Experimental Study of Powder Spreading Process in Additive Manufacturing, Powder Technology 306, 2017, 45-54.
- [16] M.Y. Shaheen, A.R. Thornton, S. Luding, T. Weinhart, The Influence of Material and Process Parameters on Powder Spreading In Additive Manufacturing, Powder Technology 383, 2021, 564-583.

- [17] L. Wang, E. Li, H. Shen, R. Zou, A. Yu, Z. Zhou, Adhesion Effects on Spreading of Metal Powders in Selective Laser Melting, Powder Technology 363, 2020, 602-610.
- [18] H. Miyanaji, S. Zhang, A. Lassell, A. Zandinejad, L. Yang, Process development of porcelain ceramic material with binder jetting process for dental applications, JOM 68(3), 2016, 831-841.
- [19] H. Miyanaji, S. Zhang, A. Lassell, A.A. Zandinejad, L. Yang, Optimal process parameters for 3D printing of porcelain structures, Procedia Manufacturing 5, 2016, 870-887.
- [20] H. Miyanaji, K.M. Rahman, M. Da, C.B. Williams, Effect of fine powder particles on quality of binder jetting parts, Additive Manufacturing 36, 2020, 101587.
- [21] S. Shrestha, G. Manogharan, Optimization of binder jetting using Taguchi method, JOM 69(3), 2017, 491-497.
- [22] E. Sheydaeian, Z. Fishman, M. Vlasea, E. Toyserkani, On the effect of throughout layer thickness variation on properties of additively manufactured cellular titanium structures, Additive Manufacturing 18, 2017, 40-47.
- [23] S. Spath, H. Seitz, Influence of Grain Size and Grain-Size Distribution on Workability of Granules With 3D Printing, The International Journal of Advanced Manufacturing Technology 70(1-4), 2014, 135-144.
- [24] I. Rishmawi, M. Salarian, M. Vlasea, Tailoring green and sintered density of pure iron parts using binder jetting additive manufacturing, Additive Manufacturing 24, 2018, 508-520.
- [25] L. Meyer, A. Wegner, G. Witt, Influence of the Ratio Between the Translation and Contra-Rotating Coating Mechanism on Different Laser Sintering Materials and Their Packing Density, Solid Freeform Fabrication Symposium, Austin, TX, US, 2017.
- [26] I. Rishmawi, M. Vlasea, Binder Jetting of Silicon Steel, Part I: Process Map of Green Density, Journal of Manufacturing Science and Engineering 143(11), 2021, 111010.
- [27] ISO, 18754 Fine Ceramics (Advanced Ceramics, Advanced Technical Ceramics)-Determination of Density and Apparent Porosity, 2003.
- [28] ASTM, C1161 Standard Test Method for Flexural Strength of Advanced Ceramics at Ambient Temperature, 2018.
- [29] W. Nan, M. Pasha, M. Ghadiri, Numerical Simulation of Particle Flow and Segregation During Roller Spreading Process in Additive Manufacturing, Powder Technology 364, 2020, 811-821.
- [30] S. Lee, Powder Layer Generation for Three Dimensional Printing, Master's thesis, Massachusetts Institute of Technology, 1992.